

This discussion paper is/has been under review for the journal Atmospheric Chemistry and Physics (ACP). Please refer to the corresponding final paper in ACP if available.

Development of an aerosol microphysical module: Aerosol Two-dimensional bin module for foRmation and Aging Simulation (ATRAS)

H. Matsui¹, M. Koike², Y. Kondo², J. D. Fast³, and M. Takigawa¹

¹Japan Agency for Marine-Earth Science and Technology, Kanagawa, Japan

²Department of Earth and Planetary Science, Graduate School of Science, University of Tokyo, Tokyo, Japan

³Pacific Northwest National Laboratory, Richland, Washington, USA

Received: 12 March 2014 – Accepted: 2 April 2014 – Published: 28 April 2014

Correspondence to: H. Matsui (matsui@jamstec.go.jp)

Published by Copernicus Publications on behalf of the European Geosciences Union.

2-D aerosol bin module, ATRAS

H. Matsui et al.

[Title Page](#)

[Abstract](#)

[Introduction](#)

[Conclusions](#)

[References](#)

[Tables](#)

[Figures](#)

[◀](#)

[▶](#)

[◀](#)

[▶](#)

[Back](#)

[Close](#)

[Full Screen / Esc](#)

[Printer-friendly Version](#)

[Interactive Discussion](#)



Abstract

Number concentrations, size distributions, and mixing states of aerosols are essential parameters for accurate estimation of aerosol direct and indirect effects. In this study, we develop an aerosol module, designated Aerosol Two-dimensional bin module for foRmation and Aging Simulation (ATRAS), that can represent these parameters explicitly by considering new particle formation (NPF), black carbon (BC) aging, and secondary organic aerosol (SOA) processes. A two-dimensional bin representation is used for particles with dry diameters from 40 nm to 10 μm to resolve both aerosol size (12 bins) and BC mixing state (10 bins) for a total of 120 bins. The particles with diameters from 1 to 40 nm are resolved using an additional 8 size bins to calculate NPF. The ATRAS module is implemented in the WRF-chem model and applied to examine the sensitivity of simulated mass, number, size distributions, and optical and radiative parameters of aerosols to NPF, BC aging and SOA processes over East Asia during the spring of 2009. BC absorption enhancement by coating materials is about 50% over East Asia during the spring, and the contribution of SOA processes to the absorption enhancement is estimated to be 10–20 % over northern East Asia and 20–35 % over southern East Asia. A clear north-south contrast is also found between the impacts of NPF and SOA processes on cloud condensation nuclei (CCN) concentrations: NPF increases CCN concentrations at higher supersaturations (smaller particles) over northern East Asia, whereas SOA increases CCN concentrations at lower supersaturations (larger particles) over southern East Asia. Application of ATRAS to East Asia also shows that the impact of each process on each optical and radiative parameter depends strongly on the process and the parameter in question. The module can be used in the future as a benchmark model to evaluate the accuracy of simpler aerosol models and examine interactions between NPF, BC aging, and SOA processes under different meteorological conditions and emissions.

ACPD

14, 10659–10699, 2014

2-D aerosol bin module, ATRAS

H. Matsui et al.

[Title Page](#)

[Abstract](#)

[Introduction](#)

[Conclusions](#)

[References](#)

[Tables](#)

[Figures](#)

◀

▶

[Back](#)

[Close](#)

[Full Screen / Esc](#)

[Printer-friendly Version](#)

[Interactive Discussion](#)



1 Introduction

Atmospheric aerosols play an important role in Earth's climate system by scattering and absorbing solar radiation (direct effects) and by modifying the microphysical properties of clouds and precipitation (indirect effects). Estimates of these direct and indirect effects remain highly uncertain and are one of the largest uncertainties in predicting climate change (Ramanathan et al., 2001; Lohmann and Feichter, 2005; Bond et al., 2013; IPCC, 2013).

Accurate estimations of these effects in a model require good representations of aerosol number concentration, size distribution, and mixing state because these parameters are essential for calculating aerosol absorption and scattering coefficients and the number concentrations of cloud droplets activated from aerosols (Jacobson, 2000; Ghan et al., 2011; Reddington et al., 2011). However, many of the existing three-dimensional aerosol models do not represent these aerosol parameters sufficiently. These models predict mass concentrations but diagnose size distributions, number concentrations, or both by assuming variable or predetermined lognormal size distributions. A model that can predict aerosol number concentration, size distribution, and mixing state is necessary to reduce the uncertainties in the estimates of aerosol contributions to climate change.

Various physical and chemical processes play important roles in controlling the number concentration, size distribution, and mixing state of aerosols in the atmosphere. New particle formation (NPF), that is, the formation of ultrafine particles (~ 1 nm in diameter) and their subsequent growth, is considered to have a large impact on aerosol number concentrations and cloud condensation nuclei (CCN) concentrations and ultimately on cloud droplet number concentrations and the indirect effects of aerosols (Kulmala et al., 2000, 2004, 2007; Spracklen et al., 2006, 2008, 2010; Merikanto et al., 2009; Makkonen et al., 2009, 2012). Aging processes (i.e., condensation, coagulation, photochemical oxidation) of black carbon (BC) particles enhance their absorption efficiency and CCN activity, and they increase the heating rate of the atmosphere and

[Title Page](#)[Abstract](#)[Introduction](#)[Conclusions](#)[References](#)[Tables](#)[Figures](#)[|◀](#)[▶|](#)[◀](#)[▶](#)[Back](#)[Close](#)[Full Screen / Esc](#)[Printer-friendly Version](#)[Interactive Discussion](#)

the wet scavenging efficiency of BC and modify the microphysical properties of clouds (Jacobson, 2000, 2001; Bond et al., 2006, 2013; Stier et al., 2006; Moteki et al., 2007). Organic aerosol (OA) formation, which has been severely underestimated in many existing three-dimensional aerosol models (Heald et al., 2005, 2011; Volkamer et al., 2006; Matsui et al., 2009a; Spracklen et al., 2011), is also important in terms of the mass concentration and CCN activity of aerosols (Kanakidou et al., 2005; Zhang et al., 2007; Hallquist et al., 2009).

In our previous studies, we developed modules for NPF, BC aging, and secondary OA (SOA) processes individually using the Weather Research and Forecasting and Chemistry (WRF-chem) model (Matsui et al., 2011, 2013a, b, 2014). These modules succeeded in explaining important aerosol properties related to number concentrations, size distributions, and mixing states of aerosols in the atmosphere. Our NPF-resolved aerosol module (Matsui et al., 2011) can calculate condensational growth and coagulation sink of nucleated particles with 20 aerosol size bins from 1 nm to 10 µm in diameter, and the module reproduced the timing of NPF events in the Beijing region of China. Our BC mixing state resolved aerosol module (Matsui et al., 2013a) calculates BC aging processes using a two-dimensional aerosol bin representation (12×10 bins) resolving both aerosol size (from 40 nm to 10 µm in diameter) and BC mixing state (pure-BC particles, BC-free particles, and 8 different internally-mixed BC particles). This module reproduced the features of BC mixing state observed by a single-particle soot photometer (SP2) during the Aerosol Radiative Forcing in East Asia (A-FORCE) aircraft campaign and was used to evaluate the impact of the treatment of BC mixing state on radiative and microphysical properties of BC over the East Asian region. Our SOA scheme (Matsui et al., 2014), which is based on the volatility basis-set approach (Donahue et al., 2006; Jimenez et al., 2009), reproduced mass concentrations and temporal variations of OA over East Asia reasonably well.

In this study, we develop an aerosol module that can calculate all three processes simultaneously. The module, designated Aerosol Two-dimensional bin module for foRmation and Aging Simulation (ATRAS), is implemented to the WRF-chem model. Few

2-D aerosol bin module, ATRAS

H. Matsui et al.

[Title Page](#)

[Abstract](#)

[Introduction](#)

[Conclusions](#)

[References](#)

[Tables](#)

[Figures](#)

[|◀](#)

[▶|](#)

[◀](#)

[▶](#)

[Back](#)

[Close](#)

[Full Screen / Esc](#)

[Printer-friendly Version](#)

[Interactive Discussion](#)



three-dimensional aerosol models can calculate NPF, BC aging, and SOA processes simultaneously (Yu et al., 2012), and to our knowledge ATRAS can calculate all these processes simultaneously with the most detailed treatment of BC aging processes. Here, we describe the ATRAS module (Sect. 2) and present the first results of its application over East Asia to examine the sensitivity of mass, number, size distributions, and optical and radiative parameters of aerosols to NPF, BC aging, and SOA processes (Sect. 3).

2 The two-dimensional bin module: ATRAS

The ATRAS module is developed using the framework of the WRF-chem model (version 3.4) (Grell et al., 2005; Skamarock et al., 2008) and is used in combination with the Model for Simulating Aerosol Interactions and Chemistry (MOSAIC) aerosol module (Fast et al., 2006; Zaveri et al., 2008) (hereinafter referred to as WRF-chem/ATRAS-MOSAIC). We used the WRF-chem/MOSAIC model in our previous studies (Matsui et al., 2009b, 2010, 2011, 2013a, b, 2014).

The ATRAS module uses a total of 128 aerosol bins (Fig. 1). A two-dimensional bin representation is used for particles with dry diameter from 40 nm to 10 µm to resolve both aerosol size and BC mixing state. As in our BC mixing state-resolved aerosol module (Matsui et al., 2013a), aerosol sizes from 40 nm to 10 µm are divided into 12 bins, and the BC mixing state is divided into 10 bins using the fraction of BC mass to total aerosol mass concentrations under dry conditions. Within this size range, the module can resolve pure-BC particles (BC mass fraction > 0.99), BC-free particles (BC mass fraction = 0), and 8 different internally-mixed BC particles (with BC mass fractions of 0–0.1, 0.1–0.2, 0.2–0.35, 0.35–0.5, 0.5–0.65, 0.65–0.8, 0.8–0.9, and 0.9–0.99). The particles from 1 to 40 nm are resolved using 8 size bins to calculate NPF. Particles in this size range are assumed to be BC free. The module therefore uses a total of 128 bins ($12 \times 10 + 8$ bins) to represent aerosol size, BC mixing state, and NPF processes. Mass concentrations of sulfate, nitrate, ammonium, BC, OA (sum of primary

[Title Page](#)[Abstract](#)[Introduction](#)[Conclusions](#)[References](#)[Tables](#)[Figures](#)[|◀](#)[▶|](#)[Back](#)[Close](#)[Full Screen / Esc](#)[Printer-friendly Version](#)[Interactive Discussion](#)

2-D aerosol bin module, ATRAS

H. Matsui et al.

[Title Page](#)

[Abstract](#)

[Introduction](#)

[Conclusions](#)

[References](#)

[Tables](#)

[Figures](#)

[|◀](#)

[▶|](#)

[◀](#)

[▶](#)

[Back](#)

[Close](#)

[Full Screen / Esc](#)

[Printer-friendly Version](#)

[Interactive Discussion](#)



ues of hygroscopicity (κ) for each aerosol species are given by Matsui et al. (2011). In Table 1, the schemes and the representation used in ATRAS-MOSAIC are summarized and compared with those of the original WRF-chem/MOSAIC model. More details of the WRF-chem/MOSAIC model and the MOSAIC module are described by 5 Fast et al. (2006) and Zaveri et al. (2008), respectively. More details about the NPF, BC aging, and SOA schemes are described by Matsui et al. (2011, 2013a, 2013b, 2014).

3 Application of ATRAS-MOSAIC to East Asia

3.1 Simulation settings

Our previous WRF-chem simulations were conducted over East Asia during the A-
10 FORCE aircraft campaign (21 March–26 April 2009) (Matsui et al., 2013a, b, 2014). In these studies, aerosol mass concentrations and number concentrations and their spatial and temporal variations were evaluated using both aircraft and surface measurements. In this study, the ATRAS-MOSAIC model is applied to this region and period. Statistics are calculated for the period from during 24 March to 26 April 2009 (34 days).
15

The simulation domain consists of an outer domain with a horizontal grid spacing of 360 km and an inner domain with a horizontal grid spacing of 120 km; there are 13 vertical layers up to 100 hPa (Fig. 2a). Because the ATRAS-MOSAIC module is computationally expensive, a relatively coarse grid resolution is used. However, our previous simulations using the same resolution reasonably well reproduced meteorological fields associated with synoptic-scale meteorological variations and resulting aerosol transport and variation processes during the A-FORCE period (Matsui et al., 2013a). The results for the inner domain are described in this paper. We use the National Centers for Environmental Prediction Final Operational Global Analysis data for initial and boundary conditions and for nudging (free troposphere only) of meteorological fields.
20
25 The meteorological schemes adopted in this study are similar to those used by Matsui et al. (2009, 2014).

2-D aerosol bin module, ATRAS

H. Matsui et al.

[Title Page](#)

[Abstract](#)

[Introduction](#)

[Conclusions](#)

[References](#)

[Tables](#)

[Figures](#)

[|◀](#)

[▶|](#)

[Back](#)

[Close](#)

[Full Screen / Esc](#)

[Printer-friendly Version](#)

[Interactive Discussion](#)



In this study, aerosol optical and radiative parameters (shown in Sect. 3.4) are calculated offline using the method of Matsui et al. (2013a). Local aerosol optical properties are calculated using the Mie theory algorithm developed by Bohren and Huffman (1998). The shell-core treatment (BHOAT) is used for internally mixed BC particles,
5 while the code for well-mixed particles (BHME) is applied to pure BC and BC-free particles (Matsui et al., 2013a). The enhancement of BC absorption (the lens effect) by coating material (other than BC) is calculated in the BHOAT. Radiative feedback of aerosols to meteorological parameters (e.g., temperature) is not considered in this
10 study. Aerosol indirect effect is considered to calculate aerosol activation and removal processes theoretically. This treatment influences cloud microphysics and distribution, but we do not focus on their changes in this study. Radiative calculations are performed for clear-sky conditions (Sect. 3.4).

Emission inventories are also similar to those of Matsui et al. (2014): the anthropogenic and volcanic emissions of Streets et al. (2003), biomass burning emissions of
15 the Global Fire Emissions Database version 3 (GFED3) (van der Werf et al., 2010), and the online biogenic emissions of the Model of Emissions of Gases and Aerosols from Nature version 2 (MEGAN2) (Guenther et al., 2006). A number median diameter of 50 nm and a standard deviation (σ) of 2.0 are assumed as the size distribution of primary aerosol emissions (Matsui et al., 2013a). Emissions of coarse particles are not
20 considered in this study.

We conduct nine model simulations (Table 2). The M10_SN simulation, which is the most detailed simulation with BC aging (M) with 10 BC mass fractions, SOA (S), and NPF (N) is used as the benchmark simulation in this study. The M08_SN, M06_SN,
25 M04_SN, and M01_SN simulations are runs with different numbers of BC mixing state bins, as well as with NPF and SOA. BC mixing state bins are divided into BC mass fractions of 0, 0–0.1, 0.1–0.2, 0.2–0.5, 0.5–0.8, 0.8–0.9, 0.9–0.99, and 0.99–1.0 in the M08_SN simulation; 0, 0–0.2, 0.2–0.5, 0.5–0.8, 0.8–0.99, and 0.99–1.0 in the M06_SN simulation; and 0, 0–0.8, 0.8–0.99, 0.99–1.0 in the M04_SN simulation. These simulations are compared with the M10_SN simulation to examine the sensitivity of the mass

2-D aerosol bin module, ATRAS

H. Matsui et al.

[Title Page](#)

[Abstract](#)

[Introduction](#)

[Conclusions](#)

[References](#)

[Tables](#)

[Figures](#)

[|◀](#)

[▶|](#)

[◀](#)

[▶](#)

[Back](#)

[Close](#)

[Full Screen / Esc](#)

[Printer-friendly Version](#)

[Interactive Discussion](#)



and number concentrations and optical and radiative parameters of aerosols to the number of BC mixing state bins. The M10_N simulation is compared with the M10_SN simulation to examine the impact of SOA processes on BC mixing state. The M01_N, M01_S, and M01 simulations are conducted to determine the impact of NPF and SOA processes on aerosol properties. The M10_SN and M01 simulations are compared to understand the overall effects of NPF, BC aging, and SOA processes on aerosol properties. The M01_S simulation is almost the same as the base simulation described in Matsui et al. (2014), except for the number of aerosol size bins (8 size bins for the simulation described in Matsui et al. (2014) vs. 12 size bins in M01_S). The computational cost for the M10_SN (M01_SN) simulation is a factor of 8 (2) greater than that for the M01 simulation in our application.

3.2 Comparison with measurements

We showed detailed validation results for various aerosol parameters obtained by surface and aircraft measurements (Fig. 2b) in our previous studies (Matsui et al., 2013a, b, 2014). Although the simulation setups in this study are not exactly the same as those in our previous studies (e.g., grid spacing, gas-phase chemistry mechanism, and amounts and size distribution of emissions), similar or better model performance is obtained for the following aerosol parameters in the benchmark M10_SN simulation (Fig. 3): BC, sulfate, and OA mass concentrations at Fukue (32.75° N, 128.68° E) and Hedo (26.87° N, 128.25° E) sites in Japan (outflow region from the Asian continent) (Matsui et al., 2013a, 2014); mass and number concentrations of BC and scattering aerosols (other than BC) and their vertical profiles, BC mixing state (the shell-to-core diameter ratio at a BC core diameter of 200 nm), and aerosol number concentrations (> 10 nm) in the boundary layer during the A-FORCE campaign (Matsui et al., 2013a, 2013b). We note that the model performance is improved for the volume concentration of scattering aerosols and the shell-to-core diameter ratio during the A-FORCE campaign by considering SOA processes (Fig. 3). Details of the measurements during A-FORCE are given elsewhere (Moteki and Kondo, 2007, 2010; Kondo et al., 2011;

2-D aerosol bin module, ATRAS

H. Matsui et al.

[Title Page](#)

[Abstract](#)

[Introduction](#)

[Conclusions](#)

[References](#)

[Tables](#)

[Figures](#)

[◀](#)

[▶](#)

[◀](#)

[▶](#)

[Back](#)

[Close](#)

[Full Screen / Esc](#)

[Printer-friendly Version](#)

[Interactive Discussion](#)



3.3 Aerosol mass and number concentrations and size distributions

The spatial distributions of period-averaged concentrations of PM_{2.5} (particulate matter smaller than 2.5 µm in diameter) in the M10_SN and M01 simulations at an altitude of about 1 km (sigma level of 0.895) are shown in Fig. 4a and b, and statistics are shown in Table 3. Period-averaged values are calculated using the data at 12:00 LT (03:00 UTC) during the simulation periods (24 March–26 April). The conclusions obtained in this section do not change even if we used the data at night (00:00 LT) (not shown). The period- and domain-averaged PM_{2.5} concentrations are 15.1 and 12.1 µg m⁻³ in the M10_SN and M01 simulations, respectively. The higher PM_{2.5} concentrations in the M10_SN simulation (about 25 % higher) are due mostly to SOA processes, because PM_{2.5} concentrations are different between the simulations with and without SOA processes (Table 3). The treatment of BC mixing state and NPF has a negligible impact on period-averaged PM_{2.5} in our simulations.

BC mass concentrations are influenced by the treatment of the BC mixing state (Table 3). BC mass concentration in the M10_SN simulation is higher than that in the M01_SN simulation because pure BC is explicitly resolved in the M10_SN simulation, whereas all BC is treated as internally-mixed particles in the M01_SN simulation, which results in higher wet removal efficiency (Matsui et al., 2013a). BC concentrations in the M08_SN and M06_SN simulations are almost the same as the concentration in the benchmark M10_SN simulation. These two simulations can explain more than 90 % of the total effect of BC mixing state (the difference in BC mass concentration between the M10_SN and M01_SN simulations) (Table 3). BC concentration in the M04_SN simulation is also generally consistent with that in the benchmark simulation: the M04_simulation can explain about 70 % of the total effect of the BC mixing state. These results suggest that the simulations with 4 or more mixing state bins can explain the actual BC mixing state effect reasonably well in terms of the BC mass concentra-

[Title Page](#)

[Abstract](#)

[Introduction](#)

[Conclusions](#)

[References](#)

[Tables](#)

[Figures](#)

[◀](#)

[▶](#)

[Back](#)

[Close](#)

[Full Screen / Esc](#)

[Printer-friendly Version](#)

[Interactive Discussion](#)



2-D aerosol bin module, ATRAS

H. Matsui et al.

[Title Page](#)[Abstract](#)[Introduction](#)[Conclusions](#)[References](#)[Tables](#)[Figures](#)[|◀](#)[▶|](#)[Back](#)[Close](#)[Full Screen / Esc](#)[Printer-friendly Version](#)[Interactive Discussion](#)

is seen mainly over the southern part of the simulation domain (Southeast Asia and southern China; Fig. 5d), where OA concentrations are high. These results show that NPF is an important factor in increasing CCN concentrations at higher supersaturations (smaller particles) over northern East Asia, whereas SOA is an important factor in increasing CCN concentrations at lower supersaturations (larger particles) over southern East Asia. This difference might also imply that NPF and SOA processes have spatially different influence on cloud microphysical properties over East Asia, though we do not focus on the indirect effects of aerosols in this study.

An increase in BC mass concentrations at an altitude of about 1 km is seen for particles around 100–500 nm in the accumulation mode when the BC mixing state is resolved (M10_SN and M04_SN in Fig. 6a). SOA processes increase OA mass concentrations around 100–500 nm with the shift of the size distribution to larger size (Fig. 6b). Total (bulk) mass concentrations of inorganic species are not particularly influenced by NPF, BC aging, or SOA processes (Table 3), but the size distributions of these species are shifted to larger size mainly owing to SOA processes (Fig. 6c). Number size distribution is influenced by both NPF and SOA processes (Fig. 6d). NPF has a large impact on number concentrations of particles less than 100 nm in diameter (e.g., compare the M01_N and M01 simulations). OA formation shifts the size distribution to larger size (e.g., compare the M01_S and M01 simulations) with the increase in the number concentrations of particles around 200–400 nm and the decrease in the number concentrations of particles around 30–100 nm. The combined effects of NPF and SOA are reflected in the benchmark simulation (M10_SN).

We focused on period-averaged contributions of individual processes in this section, but their impacts could be much larger locally and temporarily. For example, while BC concentration in the M10_SN simulation is about 20 % higher than that in the M01_SN simulation on period- and domain-average, the concentration is more than 40 % higher at certain places and times (Fig. 7). Even though the impact of a process is small on period- and domain-average (the concentration ratio of about 1.0 in Fig. 7), the process

Title Page

Abstract

Introduction

Conclusions

References

Tables

Figures

1

1

Back

[Close](#)

Full Screen / Esc

[Printer-friendly Version](#)

Interactive Discussion



can contribute to increase or decrease in mass and/or number concentrations at certain places and times (Fig. 7).

3.4 Aerosol optical and radiative parameters

Period-averaged optical and radiative parameters are calculated using the data at 12:00 LT during the simulation period (24 March–26 April). We focus on column aerosol optical depth (AOD), column absorption AOD (AAOD), single scattering albedo (SSA) at 1 km, heating rate by aerosols at 1 km, and change in downward solar flux by aerosols at the surface. The statistics are shown in Table 4.

Period- and domain-averaged AOD is increased by 12 % by SOA processes (Table 4). The impact of NPF and BC aging processes on AOD is negligible in our simulations.

The treatment of BC mixing state is important for AAOD, SSA, and heating rate. Column AAOD, the fraction of absorption (1–SSA) at 1 km, and the heating rate at 1 km are 16 %, 37 %, and 16 % higher, respectively, in the M01 simulation (domain average) than in the benchmark M10_SN simulation. The difference in absorption between the two simulations is due to two effects: (1) overestimation of the absorption enhancement by coating materials (lens effect, which increased absorption) and (2) underestimation of BC mass concentrations by efficient wet removal processes (which decreased absorption) in the M01 simulation by assuming internally mixing for all BC particles (Stier et al., 2006; Matsui et al., 2013a; Oshima et al., 2009). These effects on absorption partly cancel each other because of their opposite signs. Because the former effect is larger than the latter effect in this study, absorption in the M01 simulation is larger than that in the benchmark simulation.

Column AAOD is high over both northern and southern China (Fig. 8a). We calculated the absorption enhancement ratio by the lens effect for the M10_SN and M10_N simulations (Fig. 8b). In calculating the AAOD values with the assumption of externally-mixed BC particles, all the internally-mixed BC particles are separated into BC (externally-mixed) and non-BC (BC-free) particles. The absorption enhance-

[Title Page](#)[Abstract](#)[Introduction](#)[Conclusions](#)[References](#)[Tables](#)[Figures](#)[|◀](#)[▶|](#)[◀](#)[▶](#)[Back](#)[Close](#)[Full Screen / Esc](#)[Printer-friendly Version](#)[Interactive Discussion](#)

ment ratio is estimated to be about 50–60 % and 40 % in the M10_SN and M10_N simulations, respectively (Fig. 8b). Since the absorption enhancement ratio is about 100 % in the M01_SN simulation (not shown), the simulation without BC mixing state (internally-mixed treatment for all particles) overestimates the absorption enhancement by a factor of 2. The contribution of SOA processes (the difference in AAOD between M10_SN and M10_N) to total absorption enhancement is about 10–20 % over northern East Asia and about 20–35 % over southern East Asia (Fig. 8c). A reason of this latitudinal dependency is higher OA/BC mass ratio over southern East Asia (not shown). Another potential reason is that the amounts of coating materials are sufficiently large even without SOA processes over northern East Asia (Fig. 13 of Matsui et al., 2013a) and that the increase in coating materials by SOA may have smaller impact on the absorption enhancement over northern East Asia.

The difference in SSA between the benchmark and M01 simulations is caused by both BC aging and SOA processes. The treatment of BC mixing state increases SSA by 0.05 over northern China (30–45° N), where BC concentrations are high (Fig. 9a). The treatment of SOA processes is estimated to increase SSA by 0.02 at latitudes of 30–40° N, where both BC and OA concentrations are high, mainly owing to enhancement of the scattering coefficient (Fig. 9b).

The difference in heating rate by aerosols between the benchmark and M01 simulations is caused by two opposite effects. The treatment of the BC mixing state decreases the heating rate by 0.2 Kd^{-1} mainly over northern China (30–40° N) owing to the reduction of absorption (Fig. 9c). SOA processes increase the heating rate by 0.05 Kd^{-1} over central and southern China (20–35° N, Fig. 9d), where OA concentrations are high, because SOA processes increase the multiple scattering of radiation and the lens effect (Fig. 8c), both of which can enhance absorption.

The difference in downward solar flux at the surface between the benchmark and M01 simulations is also caused by two opposite effects. SOA processes decrease the downward flux at the surface by 10 Wm^{-2} with the maximum decrease over southern China (20–30° N, Fig. 9f) where OA concentrations are high. The treatment of BC mix-

2-D aerosol bin module, ATRAS

H. Matsui et al.

[Title Page](#)

[Abstract](#)

[Introduction](#)

[Conclusions](#)

[References](#)

[Tables](#)

[Figures](#)

[◀](#)

[▶](#)

[Back](#)

[Close](#)

[Full Screen / Esc](#)

[Printer-friendly Version](#)

[Interactive Discussion](#)



ing state increases the flux by 5 W m^{-2} with the maximum increase over central China, (Fig. 9e). The increase is because less absorption in the benchmark simulation leads to increased multiple scatterings of radiation and downward surface flux.

The spatial distributions of the combined effects of BC aging and SOA differ markedly between the heating rate and the downward flux. The cooling effect of the atmosphere ($\sim 1 \text{ km}$) is seen over northern China ($30\text{--}40^\circ \text{N}$) and over the Asian continent (Fig. 9g), whereas the negative radiative impact at the surface is seen over southern China ($20\text{--}30^\circ \text{N}$) and over the western Pacific (Fig. 9h). Because the impact of each process on each radiative parameter has a large latitudinal dependence (Fig. 9c–f), total effects also have large latitudinal dependences. Positive and negative impacts are seen for both the heating rate and the downward flux, although the warming effect around 25°N (Fig. 9g) and the positive downward flux over northern China (Fig. 9h) are not very large.

Aerosol optical and radiative parameters in the M08_SN, M06_SN, and M04_SN simulations are generally similar to those in the benchmark M10_SN simulation, although the performance deteriorates as the number of BC mixing state bins is decreased. The M06_SN and M04_SN simulations can explain 70–85 % and 60–75 % of the total BC mixing state effect (the difference in aerosol optical and radiative parameters between the M10_SN and M01_SN simulations; Table 4). These results suggest that the simulations with 4 or more mixing state bins could generally explain the actual BC mixing state effect reasonably well in terms of aerosol optical and radiative parameters in the boundary layer.

The NPF sensitivity of all the optical and radiative parameters examined in this study is small (Table 4). However, because NPF increases CCN concentrations (Sect. 3.3), this process may be of great importance in terms of the indirect effects of aerosols. SOA may also be important in estimating indirect effects because of the large sensitivity of SOA to CCN concentrations (Sect. 3.3). A simulation with a higher grid resolution is necessary to resolve finer-scale clouds and to evaluate indirect effects accurately. This type of study will be important in the future but is beyond the scope of this paper.

2-D aerosol bin module, ATRAS

H. Matsui et al.

[Title Page](#)

[Abstract](#)

[Introduction](#)

[Conclusions](#)

[References](#)

[Tables](#)

[Figures](#)

[◀](#)

[▶](#)

[Back](#)

[Close](#)

[Full Screen / Esc](#)

[Printer-friendly Version](#)

[Interactive Discussion](#)



2-D aerosol bin module, ATRAS

H. Matsui et al.

Title Page

Abstract

Introduction

Conclusions

References

Tables

Figures

◀

▶

◀

▶

Back

Close

Full Screen / Esc

Printer-friendly Version

Interactive Discussion



The sensitivities of mass, number, size distribution, and optical and radiative parameters of aerosols to NPF, BC aging, and SOA processes (discussed in Sect. 3.3 and 3.4) are shown in Fig. 10. The impact (positive or negative) and the relative importance of each process differ markedly between parameters. We calculated these complicated responses for the first time by using a detailed aerosol model that could explicitly and simultaneously represent important physical and chemical processes of aerosols. Because these responses have large spatial and temporal dependences, further application studies are needed to understand more thoroughly the importance of individual aerosol processes.

10 4 Summary and conclusions

We develop an aerosol module, Aerosol Two-dimensional bin module for foRmation and Aging Simulation (ATRAS), and implement it into the WRF-chem/MOSAIC model. This module can represent important physical and chemical processes (NPF, BC aging, and SOA) that control the number concentrations, size distributions, and mixing states of aerosols in the atmosphere. ATRAS uses a total of 128 aerosol bins (at maximum). A two-dimensional bin representation is used for particles with dry diameters from 40 nm to 10 µm in diameter to resolve both aerosol size and BC mixing state (12 × 10 bins). Particles with diameters from 1 to 40 nm are resolved using an additional 8 size bins to calculate NPF.

20 We apply ATRAS-MOSAIC to the East Asian region in spring 2009, where and when aerosol mass and number concentrations and their spatial and temporal variations have been evaluated in detail by both aircraft and surface measurements. The performance of ATRAS-MOSAIC is similar to or better than that of our previous WRF-chem/MOSAIC simulations.

25 We examine the sensitivity of mass, number, size distributions, and optical and radiative parameters of aerosols to NPF, BC aging (resolution of BC mixing state), and SOA processes by comparing the simulation results with (128 bins) and without (12 bins,

2-D aerosol bin module, ATRAS

H. Matsui et al.

[Title Page](#)[Abstract](#)[Introduction](#)[Conclusions](#)[References](#)[Tables](#)[Figures](#)[|◀](#)[▶|](#)[◀](#)[▶](#)[Back](#)[Close](#)[Full Screen / Esc](#)[Printer-friendly Version](#)[Interactive Discussion](#)

assuming internally-mixed particles) these processes. SOA processes increase PM_{2.5} and OA mass concentrations by 25 % and 300 %, respectively (period- and domain-averaged values in the boundary layer). BC mass concentrations are increased by 10–15 % by the treatment of the BC mixing state.

CCN_{1.0} and CCN_{0.1} concentrations in the boundary layer are increased by 18 % and 16 %, respectively, by both NPF and SOA processes. We find a clear north-south contrast between the impacts of NPF and SOA processes on CCN concentrations. NPF increases CCN concentrations at higher supersaturations (smaller particles) over northern East Asia, whereas SOA increases CCN concentrations at lower supersaturations (larger particles) over southern East Asia. These processes will be important for evaluation of the indirect effects of aerosols.

The detailed treatment of BC mixing state reduces the absorption coefficient because the absorption enhancement (due to the lens effect) is overestimated by a factor of 2 in the simulation without the treatment of the BC mixing state (that is, when internally mixing of BC particles is assumed). The absorption enhancement ratio by the lens effect is about 50 % in our simulation over East Asia. SOA processes increase both scattering and absorption coefficient (by the lens effect). The contribution of SOA processes to total absorption enhancement is estimated to be 10–20 % over northern East Asia and 20–35 % over southern East Asia.

BC aging processes decrease the heating rate at 1 km by 0.2 K d⁻¹ and increase the downward flux at the surface by 5 W m⁻² mainly over northern China, where BC concentrations are high. SOA processes increase the heating rate at 1 km by 0.05 K d⁻¹ and decrease the downward flux at the surface by 10 W m⁻² mainly over southern China where OA concentrations are high. As a result, the spatial distributions of the combined effects of BC aging and SOA processes differ substantially between the heating rate and the downward flux.

Sensitivity simulations show that the simulations with 4 or more mixing state bins can generally explain the actual BC mixing state effect reasonably well in terms of BC mass concentrations and aerosol optical and radiative parameters.

2-D aerosol bin module, ATRAS

H. Matsui et al.

[Title Page](#)

[Abstract](#)

[Introduction](#)

[Conclusions](#)

[References](#)

[Tables](#)

[Figures](#)

[|◀](#)

[▶|](#)

[◀](#)

[▶](#)

[Back](#)

[Close](#)

[Full Screen / Esc](#)

[Printer-friendly Version](#)

[Interactive Discussion](#)



ATRAS-MOSAIC has the potential to be a benchmark module for aerosol microphysical and chemical processes. The module can be used to understand which processes and parameters should be represented in detail and which ones can be simplified in predicting mass, number, size distributions, and optical and radiative parameters of aerosols.

The module can also be used to examine complicate interactions between aerosol processes, such as the impact of SOA on NPF and on BC aging and removal. The detailed aerosol model will be a useful tool to understand more accurately the complicated and nonlinear climatic responses of aerosol processes to the change in meteorological conditions and emissions of chemical species in the future.

Acknowledgements. This work was supported by the Ministry of Education, Culture, Sports, Science, and Technology and the Japan Society for the Promotion of Science (MEXT/JSPS) KAKENHI grant numbers 26740014 and 23221001. This work was also supported by the strategic international cooperative program of the Japan Science and Technology Agency, by the global environment research fund of the Ministry of the Environment, Japan (2A-1101),

and by the Alliance for Global Sustainability project of the University of Tokyo. The authors thank Nobuhiro Moteki (University of Tokyo), Nobuyuki Takegawa (University of Tokyo), Akinori Takami (National Institute for Environmental Studies), and Yugo Kanaya (Japan Agency for Marine-Earth Science and Technology) for providing the measurement data during the A-FORCE campaign. For a part of the simulations, we used the supercomputer systems in the

University of Tokyo and Japan Agency for Marine-Earth Science and Technology. J. D. Fast was supported by the US Department of Energy (DOE) Atmospheric System Research (ASR) program under Contract DE-AC06-76RLO 1830 at PNNL. PNNL is operated for the US DOE by Battelle Memorial Institute.

References

- Abdul-Razzak, H. and Ghan, S. J.: A parameterization of aerosol activation: 2. Multiple aerosol types, *J. Geophys. Res.*, 105, 6837–6844, doi:10.1029/1999JD901161, 2000.
- Bohren, C. F. and Huffman, D. R.: *Absorption and Scattering of Light by Small Particles*, John Wiley, Hoboken, NJ, 530 pp., 1998.

2-D aerosol bin module, ATRAS

H. Matsui et al.

[Title Page](#)[Abstract](#)[Introduction](#)[Conclusions](#)[References](#)[Tables](#)[Figures](#)[|◀](#)[▶|](#)[◀](#)[▶](#)[Back](#)[Close](#)[Full Screen / Esc](#)[Printer-friendly Version](#)[Interactive Discussion](#)

- Grell, G. A., Peckham, S. E., Schmitz, R., McKeen, S. A., Frost, G., Skamarock, W. C., and Eder, B: Fully coupled “online” chemistry within the WRF model, *Atmos. Environ.*, 39, 6957–6975, 2005.
- Guenther, A., Karl, T., Harley, P., Wiedinmyer, C., Palmer, P. I., and Geron, C.: Estimates of global terrestrial isoprene emissions using MEGAN (Model of Emissions of Gases and Aerosols from Nature), *Atmos. Chem. Phys.*, 6, 3181–3210, doi:10.5194/acp-6-3181-2006, 2006.
- Hallquist, M., Wenger, J. C., Baltensperger, U., Rudich, Y., Simpson, D., Claeys, M., Dommen, J., Donahue, N. M., George, C., Goldstein, A. H., Hamilton, J. F., Herrmann, H., Hoffmann, T., Iinuma, Y., Jang, M., Jenkin, M. E., Jimenez, J. L., Kiendler-Scharr, A., Maenhaut, W., McFiggans, G., Mentel, Th. F., Monod, A., Prévôt, A. S. H., Seinfeld, J. H., Suratt, J. D., Szmigielski, R., and Wildt, J.: The formation, properties and impact of secondary organic aerosol: current and emerging issues, *Atmos. Chem. Phys.*, 9, 5155–5236, doi:10.5194/acp-9-5155-2009, 2009.
- Heald, C. L., Jacob, D. J., Park, R. J., Russell, L. M., Huebert, B. J., Seinfeld, J. H., Liao, H., and Weber, R. J.: A large organic aerosol source in the free troposphere missing from current models, *Geophys. Res. Lett.*, 32, L18809, doi:10.1029/2005GL023831, 2005.
- Heald, C. L., Coe, H., Jimenez, J. L., Weber, R. J., Bahreini, R., Middlebrook, A. M., Russell, L. M., Jolley, M., Fu, T.-M., Allan, J. D., Bower, K. N., Capes, G., Crosier, J., Morgan, W. T., Robinson, N. H., Williams, P. I., Cubison, M. J., DeCarlo, P. F., and Dunlea, E. J.: Exploring the vertical profile of atmospheric organic aerosol: comparing 17 aircraft field campaigns with a global model, *Atmos. Chem. Phys.*, 11, 12673–12696, doi:10.5194/acp-11-12673-2011, 2011.
- IPCC: Summary for policymakers, in: Climate Change 2013: The Physical Science Basis, Contribution of Working Group I to the Fifth Assessment Report of the Intergovernmental Panel on Climate Change, edited by: Stocker, T. F., Qin, D., Plattner, G.-K., Tignor, M., Allen, S. K., Boschung, J., Nauels, A., Xia, Y., Bex, V., and Midgley, P. M., Cambridge University Press, Cambridge, UK and New York, NY, USA, 1–36, 2013.
- Jacobson, M. Z.: Development and application of a new air pollution modeling system – II. Aerosol module structure and design, *Atmos. Environ.*, 31, 131–144, 1997.
- Jacobson, M. Z.: A physically-based treatment of elemental carbon optics: implications for global direct forcing of aerosols, *Geophys. Res. Lett.*, 27, 217–220, doi:10.1029/1999GL010968, 2000.

2-D aerosol bin module, ATRAS

H. Matsui et al.

[Title Page](#)[Abstract](#)[Introduction](#)[Conclusions](#)[References](#)[Tables](#)[Figures](#)[◀](#)[▶](#)[◀](#)[▶](#)[Back](#)[Close](#)[Full Screen / Esc](#)[Printer-friendly Version](#)[Interactive Discussion](#)

2-D aerosol bin
module, ATRAS

H. Matsui et al.

[Title Page](#)[Abstract](#)[Introduction](#)[Conclusions](#)[References](#)[Tables](#)[Figures](#)[◀](#)[▶](#)[◀](#)[▶](#)[Back](#)[Close](#)[Full Screen / Esc](#)[Printer-friendly Version](#)[Interactive Discussion](#)

- Jacobson, M. Z.: Strong radiative heating due to the mixing state of black carbon in atmospheric aerosols, *Nature*, 409, 695–697, 2001.
- Jacobson, M. Z., Turco, R. P., Jensen, E. J., and Toon, O. B.: Modeling coagulation among particles of different composition and size, *Atmos. Environ.*, 28, 1327–1338, 1994.
- Jimenez, J. L., Canagaratna, M. R., Donahue, N. M., Prevot, A. S. H., Zhang, Q., Kroll, J. H., DeCarlo, P. F., Allan, J. D., Coe, H., Ng, N. L., Aiken, A. C., Docherty, K. S., Ulbrich, I. M., Grieshop, A. P., Robinson, A. L., Duplissy, J., Smith, J. D., Wilson, K. R., Lanz, V. A., Hueglin, C., Sun, Y. L., Tian, J., Laaksonen, A., Raatikainen, T., Rautiainen, J., Vaattovaara, P., Ehn, M., Kulmala, M., Tomlinson, J. M., Collins, D. R., Cubison, M. J., Dunlea, E. J., Huffman, J. A., Onasch, T. B., Alfarra, M. R., Williams, P. I., Bower, K., Kondo, Y., Schneider, J., Drewnick, F., Borrmann, S., Weimer, S., Demerjian, K., Salcedo, D., Cottrell, L., Griffin, R., Takami, A., Miyoshi, T., Hatakeyama, S., Shimono, A., Sun, J. Y., Zhang, Y. M., Dzepina, K., Kimmel, J. R., Sueper, D., Jayne, J. T., Herndon, S. C., Trimborn, A. M., Williams, L. R., Wood, E. C., Middlebrook, A. M., Kolb, C. E., Baltensperger, U., and Worsnop, D. R.: Evolution of organic aerosols in the atmosphere, *Science*, 326, 1525–1529, 2009.
- Kanakidou, M., Seinfeld, J. H., Pandis, S. N., Barnes, I., Dentener, F. J., Facchini, M. C., Van Dingenen, R., Ervens, B., Nenes, A., Nielsen, C. J., Swietlicki, E., Putaud, J. P., Balkanski, Y., Fuzzi, S., Horth, J., Moortgat, G. K., Winterhalter, R., Myhre, C. E. L., Tsigaridis, K., Vignati, E., Stephanou, E. G., and Wilson, J.: Organic aerosol and global climate modelling: a review, *Atmos. Chem. Phys.*, 5, 1053–1123, doi:10.5194/acp-5-1053-2005, 2005.
- Kanaya, Y., Taketani, F., Komazaki, Y., Liu, X., Kondo, Y., Sahu, L. K., Irie, H., and Takashima, H.: Comparison of black carbon mass concentrations observed by Multi-Angle Absorption Photometer (MAAP) and Continuous Soot-Monitoring System (COSMOS) on Fukue Island and in Tokyo, Japan, *Aerosol Sci. Tech.*, 47, 1–10, 2013.
- Kondo, Y., Sahu, L., Moteki, N., Khan, F., Takegawa, N., Liu, X., Koike, M., and Miyakawa, T.: Consistency and traceability of black carbon measurements made by laser-induced incandescence, thermal-optical transmittance, and filter-based photo-absorption techniques, *Aerosol Sci. Tech.*, 45, 295–312, 2011.
- Koo, B., Ansari, A. S., and Pandis, S. N.: Integrated approaches to modeling the organic and inorganic atmospheric aerosol components, *Atmos. Environ.*, 37, 4757–4768, 2003.
- Kuang, C., McMurry, P. H., McCormick, A. V., and Eisele, F. L.: Dependence of nucleation rates on sulfuric acid vapor concentration in diverse atmospheric locations, *J. Geophys. Res.*, 113, D10209, doi:10.1029/2007JD009253, 2008.

2-D aerosol bin module, ATRAS

H. Matsui et al.

[Title Page](#)[Abstract](#)[Introduction](#)[Conclusions](#)[References](#)[Tables](#)[Figures](#)[|◀](#)[▶|](#)[◀](#)[▶](#)[Back](#)[Close](#)[Full Screen / Esc](#)[Printer-friendly Version](#)[Interactive Discussion](#)

2-D aerosol bin module, ATRAS

H. Matsui et al.

Title Page

Abstract

Introduction

Conclusions

References

Tables

Figures

◀

▶

Back

Close

Full Screen / Esc

Printer-friendly Version

Interactive Discussion



- aerosols around Beijing in summer 2006: 2. Local and column aerosol optical properties, *J. Geophys. Res.*, 115, D22207, doi:10.1029/2010JD013895, 2010.
- 5 Matsui, H., Koike, M., Kondo, Y., Takegawa, N., Wiedensohler, A., Fast, J. D., and Zaveri, R. A.: Impact of new particle formation on the concentrations of aerosols and cloud condensation nuclei around Beijing, *J. Geophys. Res.*, 116, D19208, doi:10.1029/2011JD016025, 2011.
- Matsui, H., Koike, M., Kondo, Y., Moteki, N., Fast, J. D., and Zaveri, R. A.: Development and validation of a black carbon mixing state resolved three-dimensional model: aging processes and radiative impact, *J. Geophys. Res. Atmos.*, 118, 2304–2326, doi:10.1029/2012JD018446, 2013a.
- 10 Matsui, H., Koike, M., Takegawa, N., Kondo, Y., Takami, A., Takamura, T., Yoon, S., Kim, S.-W., Lim, H.-C., and Fast, J. D.: Spatial and temporal variations of new particle formation in East Asia using an NPF-explicit WRF-chem model: north-south contrast in new particle formation frequency, *J. Geophys. Res. Atmos.*, 118, 11647–11663, doi:10.1002/jgrd.50821, 2013c.
- 15 Matsui, H., Koike, M., Kondo, Y., Takami, A., Fast, J. D., Kanaya, Y., and Takigawa, M.: Volatility basis-set approach simulation of organic aerosol formation in East Asia: implications for anthropogenic-biogenic interaction and controllable amounts, *Atmos. Chem. Phys. Discuss.*, 14, 6203–6260, doi:10.5194/acpd-14-6203-2014, 2014.
- 20 Merikanto, J., Spracklen, D. V., Mann, G. W., Pickering, S. J., and Carslaw, K. S.: Impact of nucleation on global CCN, *Atmos. Chem. Phys.*, 9, 8601–8616, doi:10.5194/acp-9-8601-2009, 2009.
- Moteki, N. and Kondo, Y.: Effects of mixing state on black carbon measurements by laser-induced incandescence, *Aerosol Sci. Tech.*, 41, 398–417, 2007.
- 25 Moteki, N. and Kondo, Y.: Dependence of laser-induced incandescence on physical properties of black carbon aerosols: measurements and theoretical interpretation, *Aerosol Sci. Tech.*, 44, 663–675, 2010.
- Moteki, N., Kondo, Y., Miyazaki, Y., Takegawa, N., Komazaki, Y., Kurata, G., Shirai, T., Blake, D. R., Miyakawa, T., and Koike, M.: Evolution of mixing state of black carbon particles: aircraft measurements over the western Pacific in March 2004, *Geophys. Res. Lett.*, 34, L11803, doi:10.1029/2006GL028943, 2007.
- 30 Moteki, N., Kondo, Y., Oshima, N., Takegawa, N., Koike, M., Kita, K., Matsui, H., and Kajino, M.: Size dependence of wet removal of black carbon aerosols during transport from the boundary layer to the free troposphere, *Geophys. Res. Lett.*, 39, L13802, doi:10.1029/2012GL052034, 2012.

- Oshima, N., Koike, M., Zhang, Y., and Kondo, Y.: Aging of black carbon in outflow from anthropogenic sources using a mixing state resolved model: 2. aerosol optical properties and cloud condensation nuclei activities, *J. Geophys. Res.*, 114, D18202, doi:10.1029/2008JD011681, 2009.
- 5 Oshima, N., Kondo, Y., Moteki, N., Takegawa, N., Koike, M., Kita, K., Matsui, H., Kajino, M., Nakamura, H., Jung, J. S., and Kim, Y. J.: Wet removal of black carbon in Asian outflow: Aerosol Radiative Forcing in East Asia (A-FORCE) aircraft campaign, *J. Geophys. Res.*, 117, D03204, doi:10.1029/2011JD016552, 2012.
- 10 Ramanathan, V., Crutzen, P. J., Kiehl, J. T., and Rosenfeld, D.: Aerosols, climate, and the hydrological cycle, *Science*, 294, 2119–2124, 2001.
- 15 Reddington, C. L., Carslaw, K. S., Spracklen, D. V., Frontoso, M. G., Collins, L., Merikanto, J., Minikin, A., Hamburger, T., Coe, H., Kulmala, M., Aalto, P., Flentje, H., Plass-Dülmer, C., Bir-mili, W., Wiedensohler, A., Wehner, B., Tuch, T., Sonntag, A., O'Dowd, C. D., Jennings, S. G., Dupuy, R., Baltensperger, U., Weingartner, E., Hansson, H.-C., Tunved, P., Laj, P., Selle-gri, K., Boulon, J., Putaud, J.-P., Gruening, C., Swietlicki, E., Roldin, P., Henzing, J. S., Moerman, M., Mihalopoulos, N., Kouvarakis, G., Ždímal, V., Zíková, N., Marinoni, A., Bonasoni, P., and Duchi, R.: Primary versus secondary contributions to particle number concentrations in the European boundary layer, *Atmos. Chem. Phys.*, 11, 12007–12036, doi:10.5194/acp-11-12007-2011, 2011.
- 20 Schell, B., Ackermann, I. J., Hass, H., Binkowski, F. S., and Ebel, A.: Modeling the formation of secondary organic aerosol within a comprehensive air quality model system, *J. Geophys. Res.*, 106, 28275–28293, doi:10.1029/2001JD000384, 2001.
- 25 Shrivastava, M., Fast, J., Easter, R., Gustafson Jr., W. I., Zaveri, R. A., Jimenez, J. L., Saide, P., and Hodzic, A.: Modeling organic aerosols in a megacity: comparison of simple and complex representations of the volatility basis set approach, *Atmos. Chem. Phys.*, 11, 6639–6662, doi:10.5194/acp-11-6639-2011, 2011.
- 30 Simmel, M. and Wurzler, S.: Condensation and activation in sectional cloud microphysical models, *Atmos. Res.*, 80, 218–236, 2006.
- Skamarock, W. C., Klemp, J. B., Dudhia, J., Gill, D. O., Barker, D. M., Wang, W., and Pow-35 ers, J. G.: A Description of the Advanced Research WRF Version 3, NCAR Tech. Note, NCAR/TN-475+STR, Natl. Cent. Atmos. Res., Boulder, Colo, 2008.
- Spracklen, D. V., Carslaw, K. S., Kulmala, M., Kerminen, V.-M., Mann, G. W., and Sihto, S.-L.: The contribution of boundary layer nucleation events to total particle concentrations on

2-D aerosol bin module, ATRAS

H. Matsui et al.

[Title Page](#)[Abstract](#)[Introduction](#)[Conclusions](#)[References](#)[Tables](#)[Figures](#)[◀](#)[▶](#)[◀](#)[▶](#)[Back](#)[Close](#)[Full Screen / Esc](#)[Printer-friendly Version](#)[Interactive Discussion](#)

regional and global scales, *Atmos. Chem. Phys.*, 6, 5631–5648, doi:10.5194/acp-6-5631-2006, 2006.

Spracklen, D. V., Carslaw, K. S., Kulmala, M., Kerminen, V.-M., Sihto, S.-L., Riipinen, I., Merikanto, J., Mann, G. W., Chipperfield, M. P., Wiedensohler, A., Birmili, W., and Lihavainen, H.: Contribution of particle formation to global cloud condensation nuclei concentrations, *Geophys. Res. Lett.*, 35, L06808, doi:10.1029/2007GL033038, 2008.

Spracklen, D. V., Carslaw, K. S., Merikanto, J., Mann, G. W., Reddington, C. L., Pickering, S., Ogren, J. A., Andrews, E., Baltensperger, U., Weingartner, E., Boy, M., Kulmala, M., Laakso, L., Lihavainen, H., Kivekäs, N., Komppula, M., Mihalopoulos, N., Kouvarakis, G., Jennings, S. G., O'Dowd, C., Birmili, W., Wiedensohler, A., Weller, R., Gras, J., Laj, P., Sellegrí, K., Bonn, B., Krejci, R., Laaksonen, A., Hamed, A., Minikin, A., Harrison, R. M., Talbot, R., and Sun, J.: Explaining global surface aerosol number concentrations in terms of primary emissions and particle formation, *Atmos. Chem. Phys.*, 10, 4775–4793, doi:10.5194/acp-10-4775-2010, 2010.

Spracklen, D. V., Jimenez, J. L., Carslaw, K. S., Worsnop, D. R., Evans, M. J., Mann, G. W., Zhang, Q., Canagaratna, M. R., Allan, J., Coe, H., McFiggans, G., Rap, A., and Forster, P.: Aerosol mass spectrometer constraint on the global secondary organic aerosol budget, *Atmos. Chem. Phys.*, 11, 12109–12136, doi:10.5194/acp-11-12109-2011, 2011.

Stier, P., Seinfeld, J. H., Kinne, S., Feichter, J., and Boucher, O.: Impact of nonabsorbing anthropogenic aerosols on clear-sky atmospheric absorption, *J. Geophys. Res.*, 111, D18201, doi:10.1029/2006JD007147, 2006.

Streets, D. G., Bond, T. C., Carmichael, G. R., Fernandes, S. D., Fu, Q., He, D., Klimont, Z., Nelson, S. M., Tsai, N. Y., Wang, M. Q., Woo, J.-H., and Yarber, K. F.: An inventory of gaseous and primary aerosol emissions in Asia in the year 2000, *J. Geophys. Res.*, 108, 8809, doi:10.1029/2002JD003093, 2003.

Takami, A., Miyoshi, T., Shimono, A., and Hatakeyama, S.: Chemical composition of fine aerosol measured by AMS at Fukue Island, Japan, during APEX period, *Atmos. Environ.*, 39, 4913–4924, 2005.

Takami, A., Miyoshi, T., Shimono, A., Kaneyasu, N., Kato, S., Kajii, Y., and Hatakeyama, S.: Transport of anthropogenic aerosols from Asia and subsequent chemical transformation, *J. Geophys. Res.*, 112, D22S31, doi:10.1029/2006JD008120, 2007.

2-D aerosol bin module, ATRAS

H. Matsui et al.

[Title Page](#)

[Abstract](#)

[Introduction](#)

[Conclusions](#)

[References](#)

[Tables](#)

[Figures](#)

[◀](#)

[▶](#)

[Back](#)

[Close](#)

[Full Screen / Esc](#)

[Printer-friendly Version](#)

[Interactive Discussion](#)



- Takegawa, N., Moteki, N., Koike, M., Oshima, N., and Kondo, Y.: Condensation particle counters combined with a low-pressure impactor for fast measurement of mode-segregated aerosol number concentration, *Aerosol Sci. Tech.*, 47, 1059–1065, 2013.
- van der Werf, G. R., Randerson, J. T., Giglio, L., Collatz, G. J., Mu, M., Kasibhatla, P. S., Morton, D. C., DeFries, R. S., Jin, Y., and van Leeuwen, T. T.: Global fire emissions and the contribution of deforestation, savanna, forest, agricultural, and peat fires (1997–2009), *Atmos. Chem. Phys.*, 10, 11707–11735, doi:10.5194/acp-10-11707-2010, 2010.
- Volkamer, R., Jimenez, J. L., San Martini, F., Dzepina, K., Zhang, Q., Salcedo, D., Molina, L. T., Worsnop, D. R., and Molina, M. J.: Secondary organic aerosol formation from anthropogenic air pollution: rapid and higher than expected, *Geophys. Res. Lett.*, 33, L17811, doi:10.1029/2006GL026899, 2006.
- Wexler, A. S., Lurmann, F. W., and Seinfeld, J. H.: Modelling urban and regional aerosols, Part I: Model development, *Atmos. Environ.*, 28, 531–546, 1994.
- Yu, F., Luo, G., and Ma, X.: Regional and global modeling of aerosol optical properties with a size, composition, and mixing state resolved particle microphysics model, *Atmos. Chem. Phys.*, 12, 5719–5736, doi:10.5194/acp-12-5719-2012, 2012.
- Zaveri, R. A., Easter, R. C., and Wexler, A. S.: A new method for multicomponent activity coefficients of electrolytes in aqueous atmospheric aerosols, *J. Geophys. Res.*, 110, D02201, doi:10.1029/2004JD004681, 2005a.
- Zaveri, R. A., Easter, R. C., and Peters, L. K.: A computationally efficient Multicomponent Equilibrium Solver for Aerosols (MESA), *J. Geophys. Res.*, 110, D24203, doi:10.1029/2004JD005618, 2005b.
- Zaveri, R. A., Easter, R. C., Fast, J. D., and Peters, L. K.: Model for Simulating Aerosol Interactions and Chemistry (MOSAIC), *J. Geophys. Res.*, 113, D13204, doi:10.1029/2007JD008782, 2008.
- Zhang, Q., Jimenez, J. L., Canagaratna, M. R., Allan, J. D., Coe, H., Ulbrich, I., Alfarra, M. R., Takami, A., Middlebrook, A. M., Sun, Y. L., Dzepina, K., Dunlea, E., Docherty, K., DeCarlo, P. F., Salcedo, D., Onasch, T., Jayne, J. T., Miyoshi, T., Shimono, A., Hatakeyama, S., Takegawa, N., Kondo, Y., Schneider, J., Drewnick, F., Borrmann, S., Weimer, S., Demerjian, K., Williams, P., Bower, K., Bahreini, R., Cottrell, L., Griffin, R. J., Rautiainen, J., Sun, J. Y., and Zhang, Y. M.: Ubiquity and dominance of oxygenated species in organic aerosols in anthropogenically-influenced Northern Hemisphere midlatitudes, *Geophys. Res. Lett.*, 34, L13801, doi:10.1029/2007GL029979, 2007.

2-D aerosol bin module, ATRAS

H. Matsui et al.

[Title Page](#)[Abstract](#)[Introduction](#)[Conclusions](#)[References](#)[Tables](#)[Figures](#)[◀](#)[▶](#)[◀](#)[▶](#)[Back](#)[Close](#)[Full Screen / Esc](#)[Printer-friendly Version](#)[Interactive Discussion](#)

2-D aerosol bin module, ATRAS

H. Matsui et al.

Table 1. Summary of chemical schemes and representations adopted in ATRAS-MOSAIC and the original MOSAIC.

Item or chemical process	ATRAS-MOSAIC	Original MOSAIC
Aerosol emission	40 nm–10 µm (pure BC, BC-free)	40 nm–10 µm (internally-mixed)
Gas-phase chemistry	SAPRC99 with SOA precursors	CBM-Z
Photolysis	Fast-J	Fast-J
Number of total aerosol bins	128 (maximum)	8
Number of aerosol size bins	20	8
Number of mixing state bins	10 (maximum)	1
Condensation and evaporation	MOSAIC (2-D)	MOSAIC
Coagulation	Two-dimensional semi-implicit method	Semi-implicit method
Nucleation	Activation-type/kinetic nucleation (PBL ^a) and binary homogeneous nucleation (FT ^a) at 1 nm Volatility basis-set	Binary homogeneous nucleation at 40 nm Primary organic aerosol only
Organic aerosol formation	Multiple hygroscopicities for each size bin	Single hygroscopicity for each size bin
CCN activation	Fahey and Pandis (2001)	Fahey and Pandis (2001)
Aqueous-phase chemistry	Multiple mixing states for each size bin	Single mixing state for each size bin
Optical properties	Easter et al. (2004)	Easter et al. (2004)
Dry and wet deposition		

^a PBL, planetary boundary layer; FT, free troposphere.

Title Page	Abstract	Introduction
Conclusions	References	
Tables	Figures	
◀	▶	
◀	▶	
Back	Close	
Full Screen / Esc		

Printer-friendly Version
Interactive Discussion



2-D aerosol bin module, ATRAS

H. Matsui et al.

Table 2. List of model simulations.

Simulation	Number of aerosol bins	BC mixing state	NPF	SOA
M10_SN	128	On (10 bins)	On	On
M10_N	128	On (10 bins)	On	Off
M08_SN	104	On (8 bins)	On	On
M06_SN	80	On (6 bins)	On	On
M04_SN	56	On (4 bins)	On	On
M01_SN	20	Off	On	On
M01_N	20	Off	On	Off
M01_S	12	Off	Off	On
M01	12	Off	Off	Off

[Title Page](#)[Abstract](#)[Introduction](#)[Conclusions](#)[References](#)[Tables](#)[Figures](#)[|◀](#)[▶|](#)[◀](#)[▶](#)[Back](#)[Close](#)[Full Screen / Esc](#)[Printer-friendly Version](#)[Interactive Discussion](#)

2-D aerosol bin
module, ATRAS

H. Matsui et al.

Table 3. Period- and domain-averaged aerosol mass and number concentrations at an altitude of about 1 km (sigma level of 0.895) at noon.

Parameter	Unit	M10_SN	M10_N	M08_SN	M06_SN	M04_SN	M01_SN	M01_N	M01_S	M01
PM _{2.5}	$\mu\text{g m}^{-3}$	15.1	12.1	15.1	15.2	15.1	15.1	12.1	15.0	12.1
BC	$\mu\text{g m}^{-3}$	0.463	0.469	0.463	0.460	0.449	0.422	0.422	0.421	0.422
OA	$\mu\text{g m}^{-3}$	4.30	1.43	4.31	4.32	4.30	4.31	1.44	4.30	1.45
SO ₄	$\mu\text{g m}^{-3}$	3.84	3.79	3.85	3.84	3.83	3.84	3.80	3.82	3.80
NH ₄	$\mu\text{g m}^{-3}$	1.89	1.87	1.89	1.89	1.88	1.88	1.87	1.87	1.87
NO ₃	$\mu\text{g m}^{-3}$	1.72	1.71	1.71	1.71	1.69	1.68	1.68	1.68	1.68
CCN _{1.0}	cm^{-3}	2434	2409	2438	2446	2443	2469	2472	2063	2061
CCN _{0.2}	cm^{-3}	1079	968	1081	1083	1079	1088	991	1034	959
CCN _{0.1}	cm^{-3}	498	427	498	499	497	495	425	491	430

Title Page

Abstract Introduction

Conclusions References

Tables Figures

◀ ▶

◀ ▶

Back Close

Full Screen / Esc

Printer-friendly Version

Interactive Discussion



2-D aerosol bin module, ATRAS

H. Matsui et al.

Table 4. Period- and domain-averaged optical and radiative parameters at noon.

Parameter	Unit	Layer	M10_SN	M10_N	M08_SN	M06_SN	M04_SN	M01_SN	M01_N	M01_S	M01
AOD	–	Column	0.257	0.229	0.257	0.257	0.256	0.255	0.227	0.257	0.229
AAOD	–	Column	0.0120	0.0113	0.0120	0.0126	0.0128	0.0141	0.0139	0.0141	0.0139
SSA	–	PBL ^a	0.930	0.926	0.930	0.927	0.925	0.912	0.903	0.913	0.904
Heating rate	K day ⁻¹	PBL ^a	0.340	0.322	0.341	0.355	0.361	0.405	0.393	0.406	0.394
Downward flux	W m ⁻²	Surface	-29.0	-25.2	-29.0	-29.6	-29.4	-30.7	-27.5	-30.8	-27.6

^a PBL, planetary boundary layer.[Title Page](#)[Abstract](#)[Introduction](#)[Conclusions](#)[References](#)[Tables](#)[Figures](#)[|◀](#)[▶|](#)[◀](#)[▶](#)[Back](#)[Close](#)[Full Screen / Esc](#)[Printer-friendly Version](#)[Interactive Discussion](#)

2-D aerosol bin module, ATRAS

H. Matsui et al.

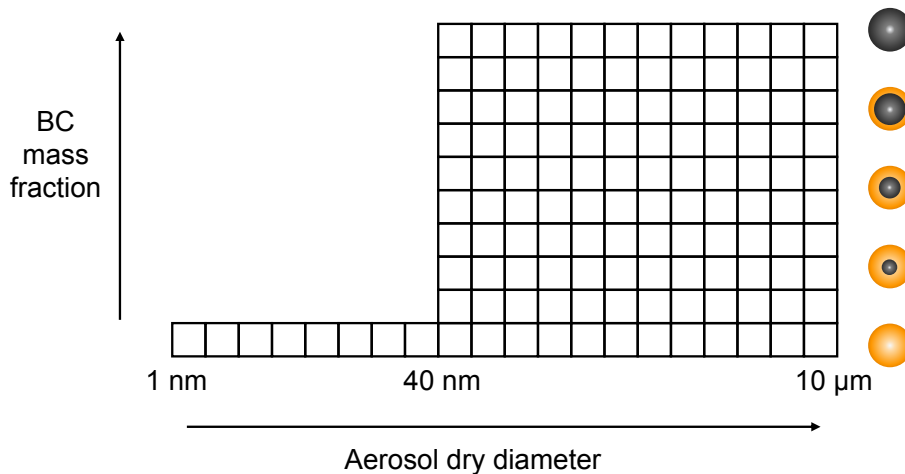


Fig. 1. Aerosol bin representation used in the ATRAS module. Particles with dry diameters from 40 nm to 10 µm are placed into two-dimensional bins. One dimension is aerosol dry diameter (12 bins from 40 nm to 10 µm), and the other is the fraction of BC mass relative to total aerosol mass concentration under dry condition (10 bins; pure-BC particles, BC-free particles, and 8 different internally-mixed BC particles). The particles with dry diameter from 1 to 40 nm are divided into 8 size bins to calculate NPF.

[Title Page](#)[Abstract](#)[Introduction](#)[Conclusions](#)[References](#)[Tables](#)[Figures](#)[|◀](#)[▶|](#)[Back](#)[Close](#)[Full Screen / Esc](#)[Printer-friendly Version](#)[Interactive Discussion](#)

2-D aerosol bin module, ATRAS

H. Matsui et al.

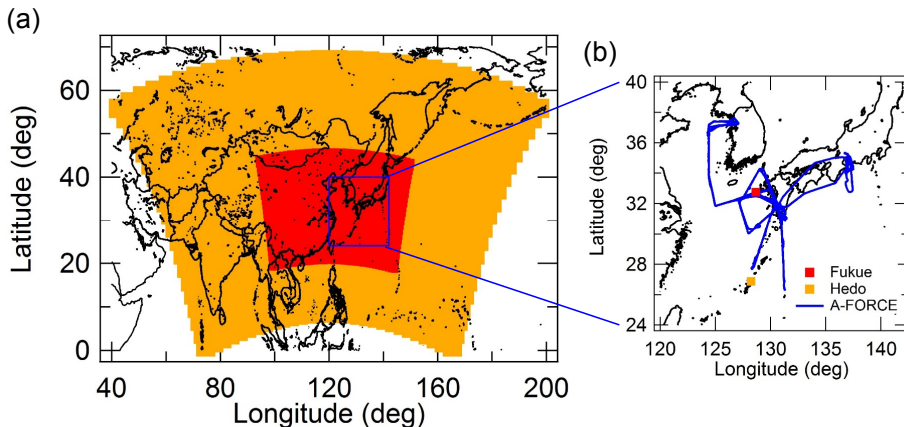


Fig. 2. (a) Simulation domain used in this study. Simulations are conducted from 21 March to 26 April 2009 with horizontal resolutions of 360 km (outer domain, orange) and 120 km (inner domain). (b) Locations of surface measurements at the Fukue and Hedo sites and flight tracks during the A-FORCE aircraft campaign, which are used to validate model simulations in this study.

Title Page	Abstract	Introduction
Conclusions	References	
Tables	Figures	
◀	▶	
◀	▶	
Back	Close	
Full Screen / Esc		

Printer-friendly Version
Interactive Discussion



2-D aerosol bin module, ATRAS

H. Matsui et al.

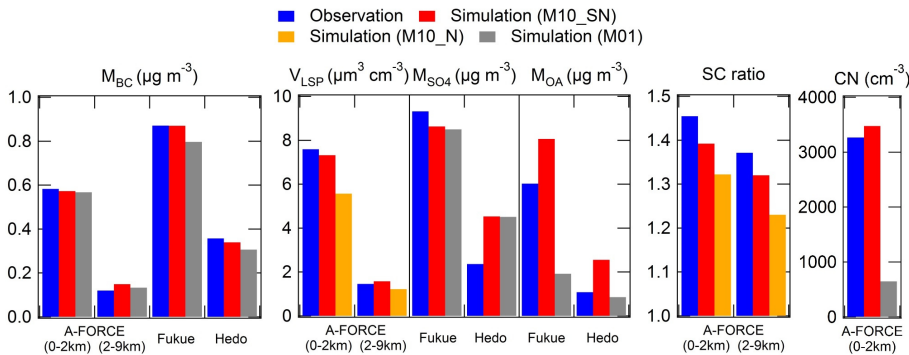


Fig. 3. Comparison of model simulation results with observed average mass concentrations of BC (M_{BC}), sulfate (M_{SO_4}), and organic aerosol (M_{OA}), volume concentration of light scattering particles (V_{LSP}), the shell-to-core diameter ratio at a BC core diameter of 200 nm (SC ratio), and number concentration of Aitken-mode particles (10–130 nm) (CN). Simulated aerosol concentrations are chosen from a horizontal and vertical grid closest to each site (for surface measurements at Fukue and Hedo) or flight track (for aircraft measurements during A-FORCE).

[Title Page](#)

[Abstract](#)

[Introduction](#)

[Conclusions](#)

[References](#)

[Tables](#)

[Figures](#)

[◀](#)

[▶](#)

[Back](#)

[Close](#)

[Full Screen / Esc](#)

[Printer-friendly Version](#)

[Interactive Discussion](#)



2-D aerosol bin module, ATRAS

H. Matsui et al.

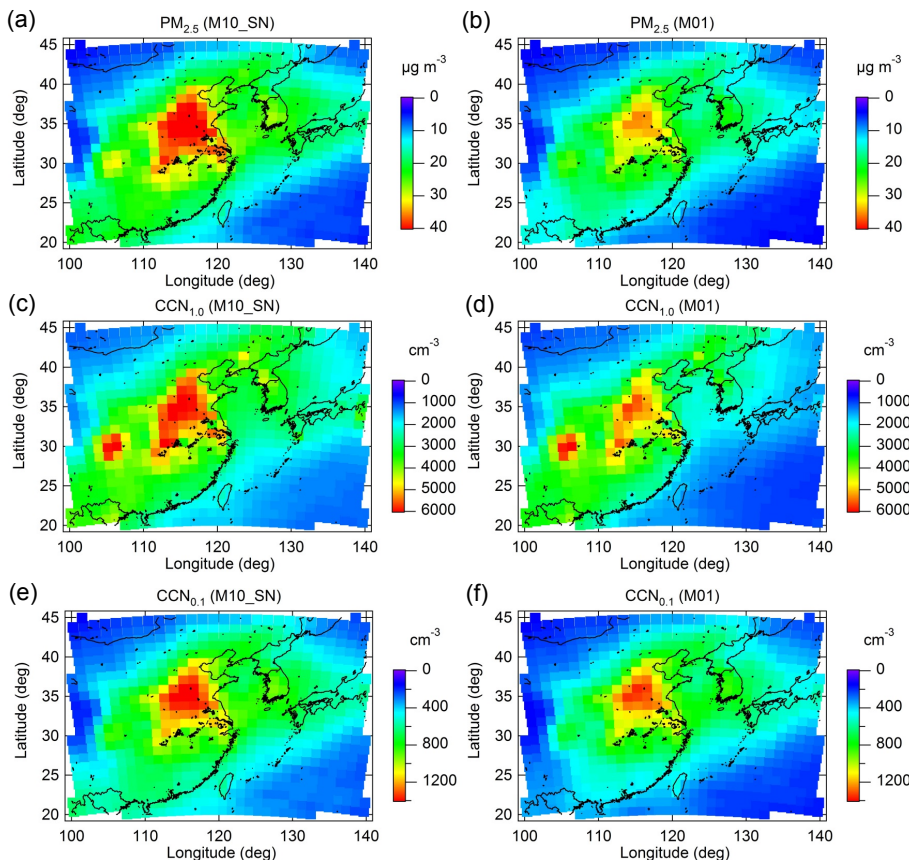


Fig. 4. Period-averaged $\text{PM}_{2.5}$ (**a** M10_SN and **b** M01 runs), CCN concentrations at supersaturations of 1% (CCN_{1.0}) (**c** M10_SN and **d** M01 runs), and CCN concentrations at supersaturations of 0.1% (CCN_{0.1}) (**e** M10_SN and **f** M01 runs) at a sigma level of 0.895 (~1 km). Period-averaged values are calculated using the data at 12:00 local time (03:00 UTC) between 24 March and 26 April.

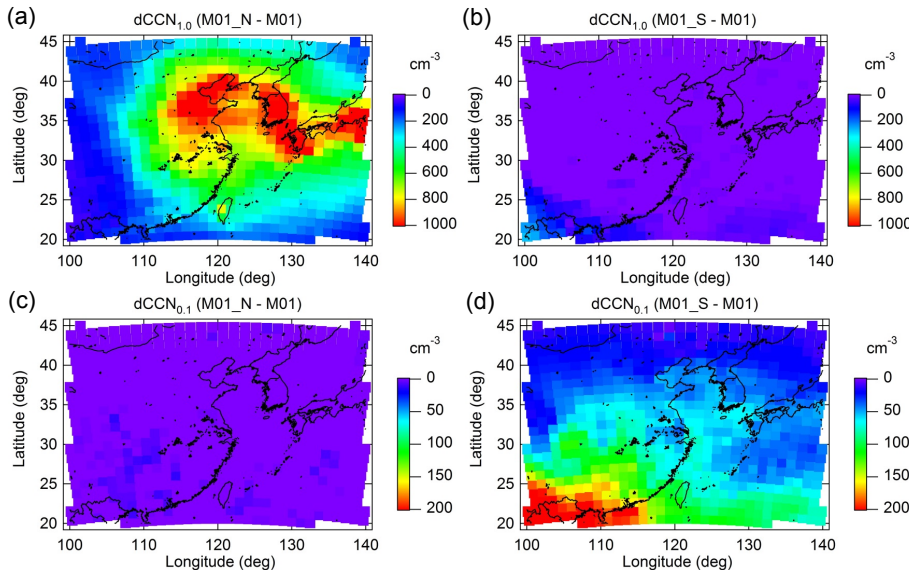


Fig. 5. Period-averaged dCCN concentrations at a sigma level of 0.895 (~1 km). dCCN is defined as the difference in CCN concentration between M01_N and M01 (left panels, **(a)** $CCN_{1.0}$ and **(c)** $CCN_{0.1}$) or between M01_S and M01 (right panels, **(b)** $CCN_{1.0}$ and **(d)** $CCN_{0.1}$). dCCN between M01_N (M01_S) and M01 can be used as a measure of the importance of NPF (SOA).

2-D aerosol bin module, ATRAS

H. Matsui et al.

[Title Page](#)

[Abstract](#)

[Introduction](#)

[Conclusions](#)

[References](#)

[Tables](#)

[Figures](#)

[|◀](#)

[▶|](#)

[◀](#)

[▶](#)

[Back](#)

[Close](#)

[Full Screen / Esc](#)

[Printer-friendly Version](#)

[Interactive Discussion](#)



2-D aerosol bin module, ATRAS

H. Matsui et al.

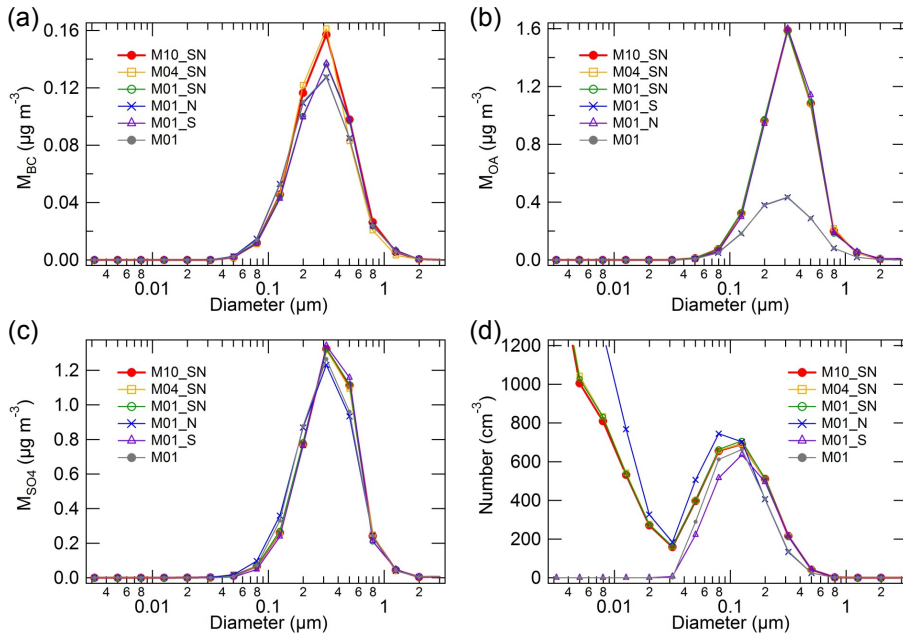


Fig. 6. Period- and domain-averaged size distributions of (a) BC, (b) OA, and (c) sulfate mass concentrations and (d) number concentrations at a sigma level of 0.895 ($\sim 1 \text{ km}$) in six simulations (the simulations are defined in Table 2).

[Title Page](#)[Abstract](#)[Introduction](#)[Conclusions](#)[References](#)[Tables](#)[Figures](#)[|◀](#)[▶|](#)[◀](#)[▶](#)[Back](#)[Close](#)[Full Screen / Esc](#)[Printer-friendly Version](#)[Interactive Discussion](#)

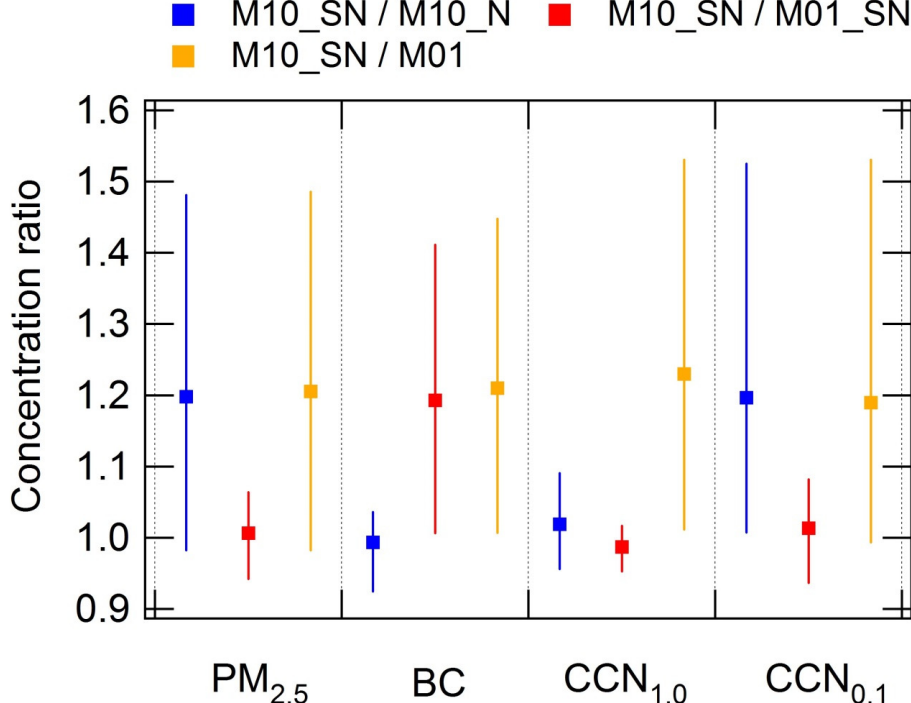


Fig. 7. Concentration ratios of $\text{PM}_{2.5}$, BC, $\text{CCN}_{1.0}$, and $\text{CCN}_{0.1}$ for the simulations between M10_SN and M10_N (blue), between M10_SN and M01_SN (red), and between M10_SN and M01 (orange). Squares show period- and domain-averaged concentration ratios at a sigma level of 0.895 (~1 km). Vertical bars show 10th–90th percentiles of concentration ratios at a sigma level of 0.895 (~1 km) for all horizontal and temporal model datasets.

2-D aerosol bin module, ATRAS

H. Matsui et al.

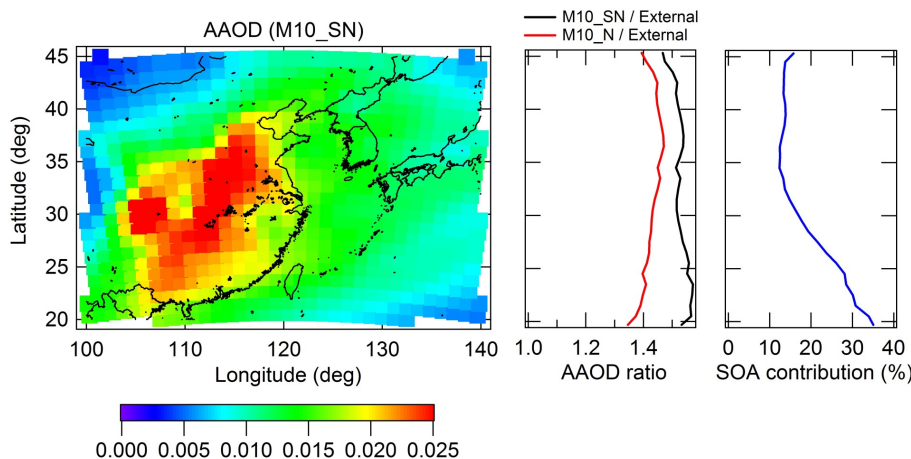
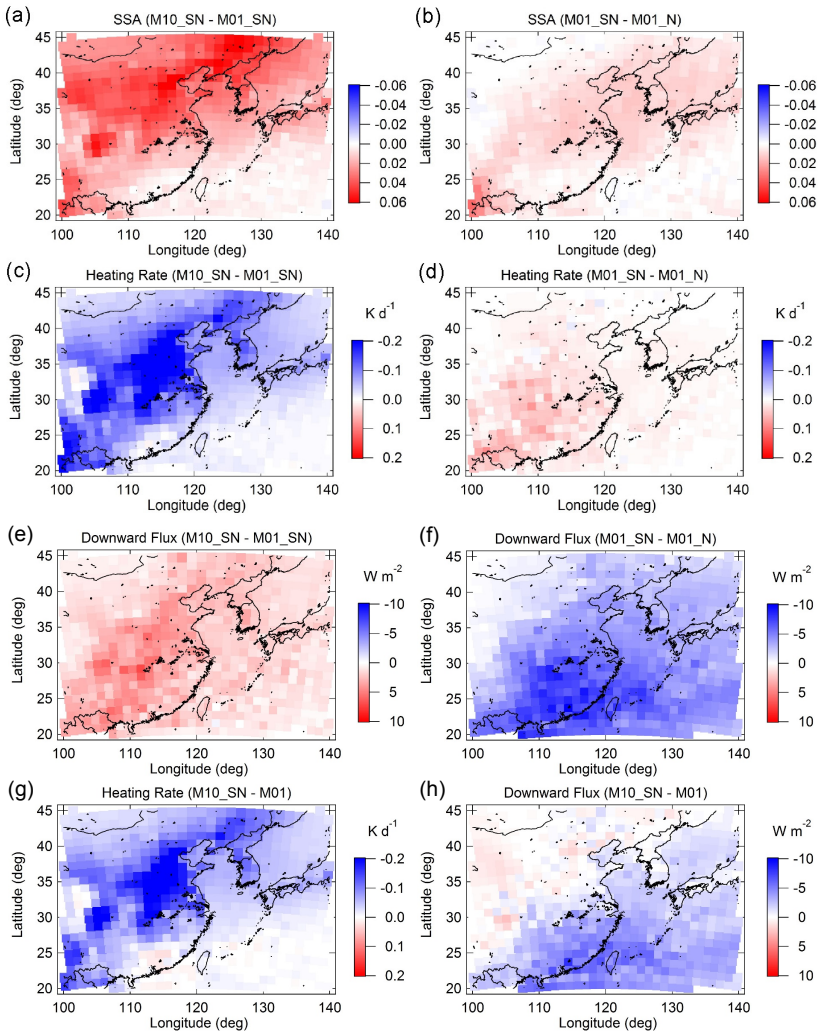


Fig. 8. **(a)** Period- and domain-averaged AAOD at a sigma level of 0.895 ($\sim 1 \text{ km}$) in the M10_SN simulation. **(b)** Latitudinal dependence of mean AAOD values in the M10_SN (black) and M10_N (red) simulations normalized by the AAOD calculated with the assumption of externally-mixed BC particles (External). In the External calculation, all the internally-mixed BC particles are separated into BC (externally-mixed) and non-BC (BC-free) particles. **(c)** Latitudinal dependence of the contribution of SOA processes to the absorption enhancement by coating materials. The contribution is calculated from two AAOD differences: the fraction of the AAOD difference between the M10_SN and M10_N simulations ($M10_{SN}-M10_N$) relative to the AAOD difference between the M10_SN simulation and the external calculation ($M10_{SN}-\text{External}$).

Title Page	Abstract	Introduction
Conclusions	References	
Tables	Figures	
Discussion Paper	Discussion Paper	Discussion Paper
I <	I >	
◀	▶	
Back	Close	
Full Screen / Esc		
Printer-friendly Version		
Interactive Discussion		

2-D aerosol bin module, ATRAS

H. Matsui et al.



[Title Page](#)

[Abstract](#)

[Introduction](#)

[Conclusions](#)

[References](#)

[Tables](#)

[Figures](#)

[◀](#)

[▶](#)

[◀](#)

[▶](#)

[Back](#)

[Close](#)

[Full Screen / Esc](#)

[Printer-friendly Version](#)

[Interactive Discussion](#)



Fig. 9. Period-averaged impacts of (left panels) BC aging and (right panels) SOA on SSA at 1 km (**a** and **b**), heating rate by aerosols at 1 km (**c** and **d**), and change in downward solar flux by aerosols at the surface (**e** and **f**). The contributions of BC aging and SOA are estimated from the difference between the M10_SN and M01_SN simulations and between the M01_SN and M01 simulations, respectively. In the bottom two panels, the combined effects of BC aging and SOA (the difference between the M10_SN and M01 simulations) are also shown for (**g**) heating rate by aerosols and (**h**) change in downward solar flux by aerosols at the surface. Period-averaged values are calculated offline using the data at 12:00 LT (03:00 UTC) between 24 March and 26 April.

2-D aerosol bin module, ATRAS

H. Matsui et al.

[Title Page](#)[Abstract](#)[Introduction](#)[Conclusions](#)[References](#)[Tables](#)[Figures](#)[|](#)[|](#)[◀](#)[▶](#)[Back](#)[Close](#)[Full Screen / Esc](#)[Printer-friendly Version](#)[Interactive Discussion](#)

2-D aerosol bin module, ATRAS

H. Matsui et al.

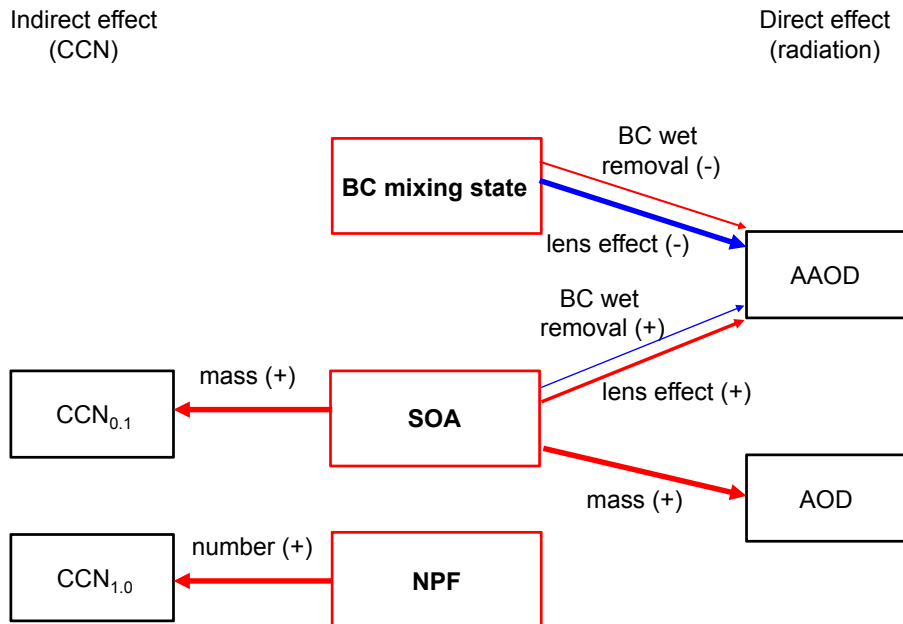


Fig. 10. Summary of the sensitivity of mass and number concentrations and optical and radiative parameters of aerosols to NPF, BC aging, and SOA. Red (blue) lines indicate positive (negative) impacts on individual aerosol parameters (black boxes). The impact of NPF (SOA) is the difference in each parameter between the simulations with and without NPF (SOA). The impact of BC aging is the difference in each parameter between when the BC mixing state is resolved and when the average mixing state is used (all BC particles are assumed to be internally-mixed).

Title Page	Abstract	Introduction
Conclusions	References	
Tables	Figures	
◀	▶	
◀	▶	
Back	Close	
Full Screen / Esc		
Printer-friendly Version		
Interactive Discussion		

